Topics in Catalysis (2018) 61:1607–1614
https://doi.org/10.1007/s11244-018-1011-5

ORIGINAL PAPER

Spectral Selective Solar Light Enhanced Photocatalysis: TiO_2/TiAlN Bilayer Films

Lars Österlund[1] · Andreas Mattsson[1] · Martin Brischetto[1] · Joel Johansson Byberg[1] · Bozhidar I. Stefanov[1] · Yu-Xia Ji[1] · Gunnar A. Niklasson[1]

Published online: 14 June 2018

Abstract
We demonstrate that spectral selective photocatalytic multilayer films can be tailored such that they can harness the full solar spectrum for enhanced photocatalytic gas-phase oxidation of acetaldehyde. Thin films of anatase TiO_2 were deposited on a thin solar absorber TiAlN film to fabricate bilayer TiO_2/TiAlN films by dc magnetron sputtering on aluminium substrates. The structural and optical properties of the films were characterized by X-ray diffraction and Raman spectroscopy. The reaction rate and quantum yield for acetaldehyde removal was measured and an almost tenfold enhancement of the quantum yield was observed for the TiO_2/TiAlN films compared with the single TiO_2 film, on par with enhancements achieved with new heterojunction photocatalysts. The results were interpreted by a temperature-induced change of the reaction kinetics. Absorption of simulated solar light illumination resulted in a temperature increase of the TIAlN film that was estimated to be at most 126 K. We show that a concomitant temperature increase of the top layer TiO_2 by 100 K shifts the water gas-surface equilibrium from multilayer to submonolayer coverage. We propose that this is the main reason for the observed enhancement of the photocatalytic activity, whereby gas phase molecules may come in direct contact with free surface sites instead of having to diffuse through a thin water film. The implications of the results for judicious control of temperature and relative humidity for efficient gas-phase photocatalysis and exploitation of selective solar absorbing films are discussed.

Keywords TiO_2 · TiAlN · Photocatalysis · Spectral selective films

1 Introduction

The indoor air is of great concern for our health. Today, we spend about 90% of our time indoors—at home, at work places, or in vehicles. It has been known for many decades that poor indoor air quality causes adverse health effects, such as the Sick Building Syndrome (SBS) [1].cc It is estimated that up to one-third of all buildings in Europe and North America are afflicted by the SBS. While the outdoor air has been the subject for many studies over the past few decades, our understanding of the indoor air chemistry and its consequences for our health is much less studied. As highlighted in a recent perspective article [2], the chemical transformation that occur in the indoor setting account for 3 of the top 10 risk factors for adverse health globally: household air pollution from solid fuels, tobacco smoking and ambient particulate matter pollution [3]. Moreover, it has been shown by recent result that chemicals which are used for occupational cleaning or domestic cleaning may lead to accelerated decline in lung function [4]. Obviously, it is essential to perform more detailed studies on the chemistries in the indoor environment to be able to characterize risk factors, and eventually eliminate them. In addition, smart ways to improve the indoor climate should be considered. For example, photocatalytic filters for indoor air treatment can reduce ventilation demands and allow for down-sizing of ventilation systems; up to 30% energy savings have been reported while down-sizing HVAC equipment by 25%—with no additional initial investment costs [5, 6].

Heterogeneous photocatalysis is an attractive method for air purification [6–9]. Light illumination of particulate metal oxides promises to provide a cost-effective and environmentally benign route to degrade pollutants, which do not require unstable and potentially dangerous chemical oxidants other

✉ Lars Österlund
lars.osterlund@angstrom.uu.se

[1] Department of Engineering Sciences, The Ångström Laboratory, Uppsala University, P. O. Box 534, 75121 Uppsala, Sweden

than oxygen in the air. A major benefit of a photocatalytic process is that it is driven by light and can activate processes that are not thermally accessible at ambient conditions. Today there exists a comprehensive understanding of the photocatalytic action of semiconducting metal oxides, and primarily TiO_2 [8, 10, 11]. While gas–solid photocatalytic reactions for air cleaning can be an order of magnitude larger than corresponding liquid–solid phase reaction for water cleaning, with quantum efficiencies of the order of 1% [6, 12], the issue of photocatalyst deactivation in gas–solid applications must be solved [13]. At the same time, it is essential that rate determining steps are identified and that new methods and materials are devised to increase the photocatalyst efficiency. Recently, methods to employ upconversion nanoparticle-based Förster resonance energy transfer (FRET) systems to convert near-infrared (NIR) light to visible and UV photons that are active for photocatalysis have been developed, thus enhancing their solar light activity [14, 15]. Other studies have explored facet-dependent reactivity of TiO_2 to enhance the intrinsic surface reaction kinetics [16].

We have previously shown that the rate determining step in the photocatalytic gas-phase degradation of hydrocarbons on TiO_2 is the oxidation of stable surface-bound intermediates [17, 18]. Indeed it is well-known that surface compounds with a carboxylic group ($R\text{-}CO_2^-$) readily form on metal oxides. In the 1960s it was even considered that organics reacted stoichiometrically with metal oxides such as TiO_2 and ZnO [19]. Albeit, we know today that the bonding of such organics is reversible, high temperature, or chemical cleaning is required for their complete removal. By adjusting reaction conditions (catalyst temperature and relative humidity) it has, however, been recognized that TiO_2 photocatalysts may become both more efficient and durable when intermediate carboxylate bonding is prevented [20–22].

In this paper we show that TiO_2/TiAlN bilayer films can utilize much of the infrared part of the solar light spectrum, thereby causing a significant increase of the film temperature that result in an almost tenfold enhancement of the quantum yield for indoor air purification. This approach is fundamentally different from upconversion nanoparticle based approaches [14, 15], and is decoupled from choice of photocatalyst material. We show that the enhancement instead is due to thermal heating of the underlying solar absorber and transfer of heat to the photocatalyst, which is accompanied by a concomitant reduction of the water coverage on the TiO_2 surfaces, which dramatically affects the reaction rate.

2 Experimental

2.1 TiO_2/TiAlN Film Preparation

TiAlN films were prepared on 50×50 mm aluminum (Al) substrates heated to about 200 °C by dc reactive magnetron sputtering using a $Ti_{0.5}Al_{0.5}$ target (99.99% purity, Plasmaterials, Livermore, CA, USA) and an argon/nitrogen ratio of 6 and a total pressure of 8 mbar, employing a Balzers UTT400 sputter system, as described elsewhere [23, 24]. Prior to deposition the protective oxide layer on the Al substrates was etched away in H_3PO_4/H_2O solution. To verify the removal of the oxide layer, reflectance was measured in the infrared region using FTIR spectroscopy (Tensor 27, Bruker Optics, Ettlingen, Germany). The thickness of the TiAlN film was measured to be 110 ± 3 nm using profilometry (Bruker DektakXT, Karlsruhe, Germany). A 102 ± 3 nm thick TiO_2 layer was subsequently sputtered on top of the TiAlN film using a Ti target (99.99% purity, Plasmaterials, Livermore, CA, USA) using a substrate temperature of ≈ 230 °C, and an oxygen-to-argon ratio of 0.045. For comparisons a TiO_2 layer with the same thickness was also deposited directly on the etched Al substrates.

2.2 Materials Characterization

The film structure was investigated by grazing-incidence X-ray diffraction (GIXRD) using $CuK_{\alpha 1}$ radiation employing a Siemens D5000 diffractometer equipped with parallel-beam optics and 0.4° Soller-slit collimator (Bruker AXS, Karlsruhe, Germany). The grazing angle was set to 1.0° and the diffractograms were collected with 1.5 s integration time and 0.02° resolution.

Raman spectroscopy was obtained with a confocal Raman microscope (inVia, Renishaw plc, Gloucestershire, UK) equipped with a 514 nm laser and 1800 groves/mm grating. Neutral density filters were used to attenuate the beam to prevent sample damage. Smoothing of the acquired spectra was done using a Savitzky-Golay filter with a three data point window.

Figure 1a shows Raman spectra of TiO_2 and TiO_2/TiAlN films on Al. The Raman spectrum of TiO_2 reveal the typical anatase E_g peak at 144 cm^{-1} as well as minor E_g, B_{1g}, $A_{1g} + B_{1g}$, and E_g peaks at ~ 197, 397, 515, and 637 cm^{-1}, respectively [25]. Similarly, the Raman spectrum of the TiO_2/TiAlN film shows bands due to anatase TiO_2, which is overlaid a broad background with resolved bands at ≈ 255 cm^{-1} due to the acoustic phonon mode in crystalline TiAlN, and at ≈ 710 cm^{-1} due to amorphous TiN_x chains, while the optical phonon mode, which overlaps the anatase E_g mode at 637 cm^{-1}, are not resolved [26, 27]. Figure 1b shows the corresponding XRD diffractograms and reveal

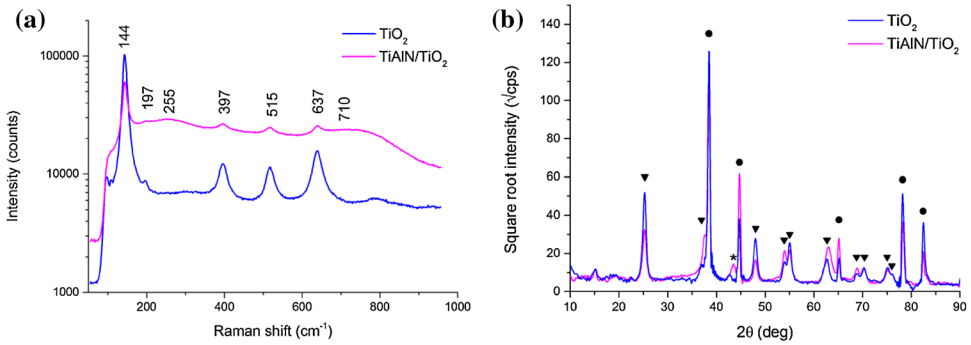

Fig. 1 **a** Raman spectra, and **b** XRD diffractograms of TiO_2 and TiO_2/TiAlN films. The peaks due to TiO_2 anatase (solid triangle; PDF card no. 021-1272), Aluminum (solid circle; PDF card no. 004-0787) and TiN (star) are marked in the figure

only the anatase TiO_2 structure with contributions from the underlying TiAlN films [24, 28]. The resulting films have about equal Ti and Al concentration, as expected from their similar sputtering yield. It is known that $Ti_{(1-x)}Al_xN$ have the same crystal structure as TiN if $x < 0.5$. The XRD peaks associated with TiN shift with addition of Al, and for an Al concentration of $x > 0.7$ the structure also changes to that of AlN [29, 30]; in our case only the TiN phase is observed. Minor contributions from broad TiN reflections, in particular at about 43° and 63° can also be discerned [27], which is consistent with the Raman spectroscopy results of a minor TiN_x contribution.

2.3 Optical Properties

The reflectance of the films was measured from 300 to 20 μm wavelength in order to determine the normal solar absorptance, α_{sol}, and normal thermal emittance, ϵ, of the films, viz.

$$R^0_{sol,therm} = \frac{\int_{sol,therm} R^0(\lambda) E_{sol,T}(\lambda) d\lambda}{\int_{sol,therm} E_{sol,T}(\lambda) d\lambda} \quad (1)$$

$$\alpha_{sol} = 1 - R^0_{sol} \quad (2)$$

$$\varepsilon(T) = 1 - R^0_{therm} \quad (3)$$

where $E_{sol,T}(\lambda)$ is the incident solar irradiance ("*sol*"), or thermal radiation spectrum ("*T*") for a black-body at temperature, T, at wavelength λ, respectively,$R^0(\lambda)$ is the bulk reflectance, and the integration is performed over the solar spectrum (0.3 μm < λ < 4.0 μm), or the measured thermal radiation region (2.5 μm < λ < 20 μm).

As seen in Table 1 the solar absorptance is about $\alpha_{sol} = 0.7$ for the pure TiAlN films, and the thermal emittance is about $\epsilon = 0.06$ at 373 K (approximate working temperature of the solar absorber film). Addition of the TiO_2 layer on top of the TiAlN does not change α_{sol} and ϵ significantly. The absorptance is higher for the TiO_2/Al than bulk TiO_2 due to absorption in the Al substrate and interference effects.

2.4 Photocatalysis Measurements

Acetaldehyde photo-degradation on TiO_2/Al and TiO_2/TiAlN samples was performed in a gas reaction cell operated in flow mode [31]. Briefly, it consists of a stainless steel body with two identical 70 mm × 70 mm glass substrates, which were mounted opposite to each other and separated by 5 mm, so that they enclose a volume of 12.5 mL. The samples were placed on the bottom glass in the reactor and were fully exposed to illumination. Acetaldehyde, CH_3CHO (90 ppm in N_2, 99.99%, Air Liquide) was mixed with synthetic air and diluted to 10 ppm, and 5 × 30 min illumination pulses, followed by 30 min purging in synthetic air between the pulses, were performed. The total flow rate was 150 ml min^{-1}. The experiments were conducted in dry gas (RH ≲ 0.5%) and at a cell temperature of 301 K. A capacitance sensor (HIH-4000, Honeywell Inc., USA), positioned in the gas stream, was used for on-line monitoring of the relative humidity. The acetaldehyde concentration, C_{CH_3CHO}, was measured in the exit gas stream by a semiconductor gas sensor (HS-130AS, Sencera Co., Taiwan) which recorded the voltage, V, across a shunt

Table 1 Thickness, solar absorptance, α_{sol}, thermal emittance at $T = 373$ K, $\epsilon(373)$, and film temperature, T_{film}, upon simulated solar light illumination ($P_{sun} = 209$ mW cm^{-2}) employing Eq. 9

Film	Thickness, d (nm)	Solar absorptance, α_{sol}	Thermal emittance, $\epsilon(373)$	T_{film} (K)
TiO_2/Al	102	0.32±0.05	0.06±0.006	54
TiO_2/TiAlN/Al	102/110	0.71±0.01	0.07±0.002	126
TiAlN/Al	110	0.72±0.01	0.06±0.005	126

resistor coupled in series with the sensing element. Data treatment of the transient responses was performed as described elsewhere [31]. The acetaldehyde concentration, $C_a(V)$ is proportional to V^2, and taking into account the baseline voltage and small amounts of residual gases remaining after each acetaldehyde pulse,

$$C_a(V) = C_{a,in}\left(\frac{(V-V_b)^2-(V_c-V_b)^2}{(V_{10}-V_b)^2-(V_c-V_b)^2}\right), \quad (4)$$

where $V_b = 0.2293V$ is the baseline voltage of the shunt resistor, V_c is the residual voltage in a purged reactor. V_{10} is the voltage in a flow of 10 ppm acetaldehyde in synthetic air. The reaction rate per unit area of the photocatalysts was then calculated as

$$k_r = F\frac{C_{a,sat-}C_{a,ss}}{AC_{a,sat}}, \quad (5)$$

where F is the molar flow rate; A is the geometrical film area which for the rather dense films is close to the true film area [16]; $C_{a,sat}$ and $C_{a,ss}$ are the measured acetaldehyde concentration at a set concentration of 10 ppm using the mass flow controllers, and at steady-state at the end of each illumination pulse, respectively. Prior to the measurements the samples were cleaned in a UV-Ozone reactor for 30 min.

In all photocatalytic measurements a Xe arc lamp (Newport, CA, USA) was employed together with a AM1.5 filter (Oriel Instruments) and a set of filters to direct and focus the light onto the samples. The measured photon power was 209 mW cm^{-2}, as measured with a thermopile detector (Ophir Optronics, Jerusalem, Israel). The total incident photon power above the measured bandgap energy of the TiO_2 films ($E_g \gtrsim 3.3$ eV, or $\lambda_g \lesssim 371$ nm) was calculated to be about 5 mW cm^{-2}. The differential quantum yield, φ, was calculated from the measured acetaldehyde photodegradation rates, viz.

$$\phi = \frac{k_r N_A}{\mathcal{F}_{ph}}, \quad (6)$$

where k_r is the rate in units of mole s^{-1}, N_A is Avogadros constant and $\mathcal{F}_{ph}$ is the absorbed photon flux (photons s^{-1}). The absorbed photon flux in the 102 nm TiO_2 films was calculated to be 4.0×10^{15} photons cm^{-2} s^{-1}, respectively, using Eq. (7):

$$\mathcal{F}_{ph} = T_g\int_0^{\lambda_g}\alpha(\lambda)E(\lambda)d\lambda, \quad (7)$$

where $T_g = 0.92$ is the transmittance through the cover glass of the cell, $\alpha(\lambda)$ is the absorption coefficient calculated from the measured reflectance data and film thicknesses, as described elsewhere [32] and (λ) is the photon flux from the lamp.

Table 2 The photo-degradation rate, k_r, and differential quantum yield, φ, on TiO_2 and TiO_2/TiAlN films. The errors are the standard deviation from 3 to 5 repeated measurements

Film	d (nm)	k_r($\times10^{-3}$ nmole cm^{-2} s^{-1})	φ ($\times10^{-3}$)
TiO_2	102	0.6±0.3	0.10±0.05
TiO_2/TiAlN	102/110	5.2±0.9	0.85±0.09

3 Results and Discussion

3.1 Reaction Rate and Quantum Yield

Table 2 shows the reaction rates (Eq. 5) and quantum yield (Eq. 6) for photocatalytic acetaldehyde photo-degradation on a double layer TiO_2/TiAlN/Al solar absorber film upon solar light illumination. As a reference the corresponding data for TiO_2/Al films are also shown. The acetaldehyde photo-degradation rate, k_r, on the TiO_2/Al film is similar to the value which can be extracted from the data reported by Papadimitriou et al. [33], albeit detailed data on e.g. photon power and illumination conditions are missing in this study. In contrast, values for the quantum yield should be independent on experimental setup and suitable for comparisons with published data. Most often data on quantum yield is, however, not reported and rather the quantum efficiency, or formal quantum efficiency (FQE), is used, where the rate is normalized to the incident photon flux. By definition ϕ is always higher than FQE, but for bandgap illumination of TiO_2 where the absorption coefficient is high, ϕ is not much higher than FQE. Nevertheless, our value of ϕ for the TiO_2/Al film is about the same as FQE for P25 powders (the most commonly used reference TiO_2 photocatalyst), and > 10 times higher than the Pilkington Activ^{TM} TiO_2 coating on glass [34], while ϕ for the TiO_2/TiAlN solar absorber film is almost 6 times higher than reported values of FQE for P25 powders and > 100 times higher than Activ^{TM} TiO_2. The similarity of FQE for P25 TiO_2 and ϕ for the TiO_2/Al film suggest that the sputtered TiO_2 films do not exhibit different intrinsic electronic properties regarding photo-excitation and recombination as crystalline TiO_2 nanoparticles. Moreover, the difference of ϕ for the double layer TiO_2/TiAlN film and a single TiO_2/Al film seen in Table 2 (more than 8 times higher on the TiO_2/TiAlN film) cannot be explained by structural differences of the TiO_2/Al and TiO_2/TiAlN films; both have very similar structure (Sect. 1.2) and surface roughness (of the order ~ 1 nm [16]). Instead, the collected data suggest that the different film temperatures under solar illumination due different

solar absorptance, shown in Table 1, for the single and multilayer films must be considered to explain the k_r and ϕ data.

3.2 Effect of Solar Energy Heating

The thin TiAlN solar absorber film absorbs > 70% of the solar light and is readily heated under solar illumination. An estimate of the solar light induced temperature increase of the TiO_2/TiAlN film can be made with reasonable assumptions about the film. We assume a free surface with constant α_{sol}, and thermal emittance, ϵ, from Table 1. The stagnation temperature in vacuum, T_s, is then given by

$$T_s = \left(T_a^4 + \frac{\alpha_{sol} P_{sun}}{\varepsilon \sigma} \right)^{1/4}, \tag{8}$$

where $T_a$is the ambient temperature, P_{sun} is the incident photon power and σ is Stefan–Boltzmann's constant. Heat loss by convection will reduce T_s. In the acetaldehyde photocatalysis reactor, the flow rate of 150 mL/min and the reactor dimension (L ~70 mm) with a reactor volume of 12.5 cm^3, yields a fluid velocity of about 2 cm/s. Thus with Reynolds number, $Re = 10$ for air and Prandtl number, $Pr = 0.7$ for air at 300 K, and using the Nusselt number,$Nu = hL/k$, where k is the heat conductivity of air ($k = 2.6 \times 10^{-2}$ W/mK for air at 300 K), we obtain [35], $Nu = 2 + 0.493Re^{0.5} \approx 4$, and hence $h \approx 11$ W/m^2K, which is in the range for natural convection (5–25 W/m^2K). For small temperature increases we can linearize the radiation term in Eq. 8 and obtain

$$\Delta T = T_s - T_a = \frac{\alpha_{sol} P_{sun}}{\varepsilon \sigma T_a^3 + h} \tag{9}$$

Equation 9 is a rough estimation of the film temperature neglecting e.g. heat conduction through sample support. The right column in Table 1 shows the estimated steady-state film temperatures for well isolated (free-hanging) TiO_2, TiO_2/TiAlN and TiAlN films on Al. It is evident that a temperature increase of more than 100 degrees can be realized on the thin TiAlN solar absorbing film, which under steady-state conditions also will be the temperature of the overlaid TiO_2 film. In contrast, the TiO_2 absorbs only in the UV part of the solar spectrum, with contributions from the Aluminium substrate (α_{sol} 0.1), and the concomitant solar heating of the single TiO_2 film is much less. These results suggest that the reaction kinetics on TiO_2 will be significantly modified, as we discuss in more detail in the next section.

3.3 Water Coverage and Reaction Mechanism

The observed enhancement of φ on the TiO_2/TiAlN double layer film compared to the single TiO_2 film can be understood by considering the temperature increase caused by the absorbed heat in the underlying TiAlN film upon solar light illumination. Two distinctly different effects of the temperature induced film heating can be distinguished. First, for thermally activated reactions, where the reaction kinetics is governed by the Arrhenius factor ($e^{-E_a/kT}$), as a rule of thumb, the reaction rate doubles for a 10 K temperature increase. In the photo-induced degradations studies here, no reactions take place without bandgap illumination, and merely increasing the temperature of the catalysts without illumination about 100 K does not result in any chemical reaction. In contrast, since desorption is normally the rate limiting step in low temperature catalysis, an increased film temperature may indirectly contribute to an overall increased reaction rate due to an enhanced the desorption rate of reaction products, which can free sites for acetaldehyde adsorption.

Another more subtle effect can also be realized by considering the influence of water coverage. The water adsorption–desorption equilibrium on TiO_2 is shifted from multilayer to submonolayer coverages around room temperature. Assuming zeroth-order water adsorption,

$$k_{ad} = s_0 \upsilon, \tag{10}$$

where

$$\upsilon = \frac{p}{\sqrt{2\pi mkT}} = 2.63 \times 10^{24} p(MT)^{-1/2}, \tag{11}$$

is the rate of impinging water molecules from the gas-phase (molecules/m^2s), p is the water pressure (in Pa), M is the water molar mass, and s_0 is the sticking coefficient which here is assumed to be $s_0 = 1$. In equilibrium we have

$$k_{ad} = k_{des}. \tag{12}$$

We assume that water desorbs according to

$$k_{des} = N_{H2O} \upsilon_0 e^{-E_{des}/RT}, \tag{13}$$

where E_{des} is the desorption energy of water, $N_{H2O}$is the number of water molecules/m^2., R is the gas constant, and υ_0 is the pre-exponential factor, which we set to $\upsilon_0 = 10^{13} s^{-1}$. Combining Eqs. 10–13, we obtain

$$N_{H2O} = 2.63 \times 10^{11} p(MT)^{-\frac{1}{2}} / e^{-E_{des}/RT} \tag{14}$$

Defining one monolayer (ML) of water to be $N_{H2O}(1ML) \equiv N_{ML} = 1.15 \bullet 10^{19}$ molecules/m^2,[36] the water coverage, θ_{H2O}, is

$$N_{H2O}/N_{ML} \equiv \theta_{H2O} = 2.287 \times 10^{-8} p(MT)^{-\frac{1}{2}} / e^{-\frac{E_{des}}{RT}}. \tag{15}$$

Equation 15 can be rewritten in terms of relative humidity (RH). At 293 K the saturation water pressure is 2338 Pa and Eq. 15 then becomes (with RH in %):

$$\theta_{H2O}(T;RH) = 5.347 \times 10^{-7} \times RH(MT)^{-\frac{1}{2}} / e^{(-E_d es/RT)}. \tag{16}$$

We can distinguish three regimes with different desorption energy for water. At θ > 2 ML, the vaporization energy of water at 298 K can be used (44 kJ/mole [37, 38]). At coverages 1 < θ < 2 ML, it has been reported that water is bonded stronger in a bilayer configuration, with desorption energy of about 48 kJ/mole [39, 40]. Finally, at θ < 1 ML the desorption energy of water from the (101) anatase surface has been estimated from temperature-programmed desorption measurements to be about 63 kJ/mole (and slightly coverage-dependent) [40]; similar values have been given for anatase nanoparticles from calometric measurements (about 62 kJ/mole) [41], while calculations have predicted lower values (52–59 kJ/mole in the low-coverage regime at θ < 0.5 ML) [42].

Figure 2a shows that in dry air (RH ≤ 0.5%) multilayers (> 2 ML) of water build up on the surface below 300 K, where desorption is governed by the heat of vaporization of liquid water. In the temperature interval 300 < *T* < 380 K water is bonded in a bilayer configuration, and above this temperature from about 380 K to about 440 K submonolayer of water exists on the surface. At even higher temperatures the surface becomes completely dehydrated. Figure 2b shows that at higher relative humidity, up to RH = 10%, the bilayer region is extended to about 390 K, and complete dehydration occurs only above about 600 K (not shown in Fig. 2b). In Fig. 3, the data in Table 2 for φ and the temperature dependence of the water coverage, shown in Fig. 2a, are combined. In Fig. 3 it is clearly seen that the increased surface temperature dramatically changes the equilibrium water coverage on the TiO_2 surfaces. At low temperature multilayers of water exist and a situation arises where diffusion of pollutants and radicals across the water film is rate determining [22]. The large enhancement of φ for the

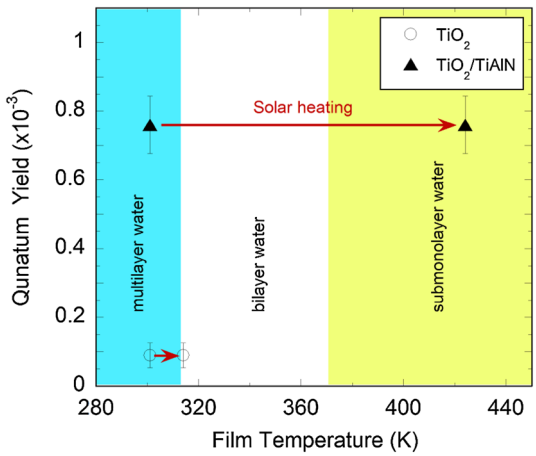

Fig. 3 Quantum yield at different film temperatures for TiO_2 and TiO_2/TiAlN double layer films. The arrows indicate the change of film temperature as a result of solar illumination (200 mw cm^{-2}), which brings results in a concomitant changed equilibrium water coverage. The blue, white and yellow regions indicate the temperature regions for multilayer, bilayer and submonolayer water coverage, respectively

TiO_2/TiAlN double layer film is directly correlated with a dramatic decrease of the equilibrium water coverage on the illuminated TiO_2/TiAlN film, which brings the water from multilayer to submonolayer coverage. Our data thus supports a mechanism where acetaldehyde photodegradation is diffusion limited at low film temperatures (around room temperature), which corresponds to most practical situation for photocatalytic air purification. A dramatic increased photocatalytic activity on the TiO_2/TiAlN double layer film under solar light illumination (about 2 Suns in our experiments) is thus a result of decreased water coverage, which is

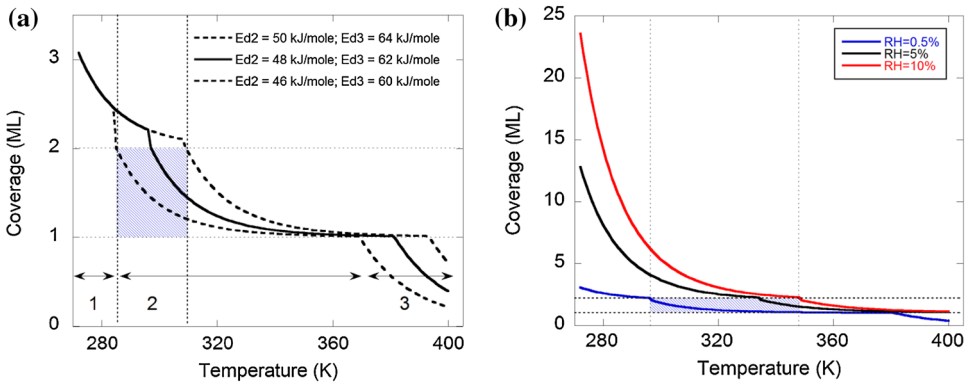

Fig. 2 **a** Water coverage as a function of surface temperature in dry air (RH = 0.5%) using reported values of desorption energies for water bonded to the TiO_2 surface at submonolayer coverage (E_{des} = 62 kJ/mole), at bilayer coverage (E_{des} = 48 kJ/mole), and multilayer coverage (E_{des} = 44 kJ/mole; i.e. the heat of vaporization). The dashed lines indicate regions of water coverage allowing for ± 2 kJ/mole variation in E_{des} from TiO_2 at submonolayer and bilayer coverages. **b** Water coverage as a function of surface temperature at different RH with water desorption energies as in (**a**). The horizontal dashed lines indicate regions of bilayer water, the vertical dashed lines regions where multilayer water is expected to build up, and the light blue region the temperature interval separating multi- and bilayer water coverages

further enhanced by an enhanced desorption rate of reaction products due to an increased surface temperature.

The mechanism for photo-oxidation of organics on TiO_2 has been attributed to either direct hole oxidation [43], or OH radical reaction [44]. If water is required as hole acceptor to generate OH radicals it is vital that not all water is desorbed from the surface, which would results in a decreased reactivity and gradual deactivation of the photocatalyst [13, 18]. An interesting implication of this model is that for a given film temperature and relative humidity, and hence a given equilibrium water coverage, it is possible to adjust either the relative humidity or the surface temperature to reach an optimum water coverage, which according to Fig. 3 should be in the submonolayer regime; it is apparent that such optimization can increase the photocatalytic activity by approximately an order of magnitude, which is on par with, or better than, the best TiO_2 photocatalyst dopant schemes, or new catalyst materials [45].

4 Conclusions

We have shown that spectral selective multilayer coatings that efficiently utilize different wavelength regions of the solar light spectrum can enhance the photocatalytic efficiency of gas–solid reactions. In particular, we have shown that a thin TiO_2 film can be sputtered on a TiAlN solar absorber film to make a double layer TiO_2/TiAlN film, which exhibits an almost tenfold enhancement of the reaction rate and quantum yield for gas-phase acetaldehyde photo-degradation in a flow through reactor. Upon simulated solar light illumination, employing 200 mW cm^{-2}, the temperature of the double layer TiO_2/TiAlN film is increased by more than 100 K. Such a temperature increase modifies that water coverage, which decreases from multilayers at room temperature to submonolayers above about 390 K in dry conditions (RH < 0.5%). When a TiO_2/TiAlN double layer is illuminated with solar light, the UV part of the spectrum is absorbed in the TiO_2 layer to create electron–hole pairs which react with acetaldehyde at the interface, either directly or via radicals, especially OH radicals. We propose that the main reason for the observed enhancement of the photocatalytic activity is due to depletion of the water from the surface, which facilitates access to free surface sites at the photocatalyst surface without the need to diffuse through a water layer. We conjecture that the same principle can be used in other multilayer configurations, e.g. photocatalytic/thermochromic, and by judicious control of the temperature and relative humidity, to achieve superior air purification performance of photocatalytic air cleaning devices.

Acknowledgements This work has received funding from the Swedish Research Council, Grant Agreement No. 2016–05904, and European Research Council under the European Community's Seventh Framework Program (FP7/2007–2013)/ERC, Grant Agreement No. 267234 ("GRINDOOR").

References

1. WHO (1983) Indoor air pollutants: exposure and health effects, vol 78.World Health Organization, Geneva
2. Gligorovski S, Abbatt JPD (2018) Science 359:632–633
3. Lim SS et al (2012) The Lancet 380:2224–2260
4. Svanes O et al Am J Respir Crit Care Med https://doi.org/10.1164/rccm.201706-1311OC
5. SD ATHP., J. FW (2005) Evaluation of ultra-violet photocatalytic oxidation (UVPCO) for indoor air applications: conversion of volatile organic compounds at low part-per-billion concentrations, LBNL-58936. Lawrence Berkeley National Laboratory, Berkley
6. Peral J, Domenech X, Ollis DF (1997) J Chem Technol Biotechnol 70:117–140
7. Hoffmann MR, Martin ST, Choi W, Bahnemann DW (1995) Chem Rev 95:69–96
8. Fujishima A, Zhang X, Tryk D (2008) Surf Sci Rep 63:515–582
9. Zhao J, Yang X (2003) Build Environ 38:645–654
10. Serpone N, Emeline AV (2012) J Phys Chem Lett 3:673–677
11. Kisch H (2013) Angew Chem Int Ed 52:812–847
12. Mills A, Le Hunte S (1997) J Photochem Photobiol A 108:1–35
13. Peral J, Ollis DF (1997) J Molec Catal A 115:347–354
14. Wang W-N et al (2018) Appl Catal B 224:854–862. https://doi.org/10.1016/j.apcatb.2017.11.037
15. Zhang F et al (2016) ChemSusChem 9:1449–1454. https://doi.org/10.1002/cssc.201600334
16. Stefanov BI, Niklasson GA, Granqvist CG, Osterlund L (2015) J Mater Chem A 3:17369–17375
17. van der Meulen T, Mattson A, Österlund L (2007) J Catal 251:131–144
18. Österlund L (2009) Vibrational spectroscopy of pure and doped TiO_2 photocatalysts. In: vayssieres L (ed) On solar hydrogen and nanotechnology. Wiley, Singapore
19. Davydov AA (2003) Molecular spectroscopy of oxide catalyst surfaces. Wiley, Chichester
20. Kozlov DV (2003) Russian Chem Bull Int Ed 52:1100–1105
21. Hägglund C, Kasemo B, Österlund L (2005) J Phys Chem B 109:10886–10895
22. Österlund L (2006) SPIE Newsroom. https://doi.org/10.1117/2.1200608.0328
23. Le Bellac D, Niklasson GA, Granqvist CG (1995) J Appl Phys 77:6145–6151
24. Zhu D, Mao F, Zhao S (2012) Solar Energy Mater Solar Cells 98:179–184
25. Ohsaka T, Izumi F, Fujiki Y (1978) J Raman Spectrosc 7:321–324
26. Barshilia HC, Rajam KS (2004) J Mater Res 19:3196–3205
27. Denisov V et al (2012) J Nano Electron Phys 4:01021
28. Powder Diffraction Files, Database Edition (2012) International Center for Diffraction Data (ICDD), Newton Square. PA 19073 – 3273
29. Hsu C-H, Chen M-L, Lai K-L (2006) Mater Sci Eng A 421:182–190

30. Man BY, Guzman L, Miotello A, Adami M (2004) Surf Coat Technol 180–181:9–14
31. Stefanov BI, Niklasson GA, Granqvist CG, Osterlund L (2016) J Catal 335:187–196
32. Topalian Z, Niklasson GA, Granqvist CG, Österlund L (2009) Thin Solid Films 518:1341–1344
33. Papadimitriou VC et al (2011) Thin Solid Films 520:1195–1201
34. Mills A et al (2003) J Photochem Photobiol A 160:213–224
35. Yuge T (1960) J Heat Transf 82:214–220
36. Diebold U (2003) Surf Sci Rep 48:53–229
37. Haynes WM, Lide DR, Bruno TJ, Press CRC (2013) CRC handbook of chemistry and physics: a ready-reference book of chemical and physical data
38. Ranea VA et al (2004) Phys Rev Lett 92
39. Henderson MA (1996) Langmuir 12:5093–5098
40. Herman GS, Dohnalek Z, Ruzycki N, Diebold U (2003) J Phys Chem B 107:2788–2795
41. Levchenko AA et al (2006) Chem Mater 18:6324–6332
42. Harris LA, Quong AA (2004) Phys Rev Lett 93:086105
43. Ishibashi K, Fujishima A, Watanabe T, Hashimoto K (2000) J Photochem Photobiol A 134:139–142
44. Sun LZ, Bolton JR (1996) J Phys Chem 100:4127–4134
45. Wang X et al (2014) J Catal 310:100–108